Contemporary Mathematics
https://ojs.wiserpub.com/index.php/CM/

Research Article

Modeling and Position Control of a Marine Vehicle with Omnidirectional Configuration

Luis F. López-Cortés[1], Yair Lozano-Hernández[2,3*], Lizeth Torres[4], Victor G. Sánchez-Meza[5], Erick Velazquez-Lozada[6]

[1] Subdirectorate of Research and Graduate Studies, Aeronautical University in Queretaro, Queretaro, Mexico
[2] Interdisciplinary Professional Unit of Engineering "Alejo Peralta" (UPIIAP), National Polytechnic Institute (IPN), Puebla, Mexico
[3] Interdisciplinary Professional Unit of Engineering, Campus Hidalgo (UPIIH) National Polytechnic Institute (IPN), Hidalgo, Mexico
[4] Institute of Engineering, National Autonomous University of Mexico (IIUNAM), Mexico City, Mexico
[5] Interdisciplinary Professional Unit of Engineering and Advanced Technologies (UPIITA), National Polytechnic Institute (IPN), Mexico City, Mexico
[6] Superior School of Mechanical and Electrical engineering, unit Zacatenco (ESIME Zacatenco), National Polytechnic Institute (IPN), Mexico City, Mexico
E-mail: ylozanoh@ipn.mx

Received: 5 December 2024; **Revised:** 6 January 2025; **Accepted:** 17 January 2025

Abstract: One of the main means of monitoring aquatic bodies are buoys, most of which are fixed, so they are not flexible enough to perform tasks such as: cleaning; rescue; exploration and surveillance. Therefore, this work is dedicated to the mathematical modeling and design of control schemes for a compact buoy with omnidirectional configuration to move between two desired points in a given time; this configuration allows the buoy to converge accurately and quickly to desired positions and routes, however, disturbances due to waves must be considered, which directly affect the movement of the buoy. These disturbances can be compensated by a robust motion controller. Thus, the dynamic model of the buoy is obtained and two control schemes are developed: Proportional-Derivative-Plus controller and Backstepping controller. These controllers base their design on a Lyapunov candidate function, which guarantees the stability of the system; however, they depend on the parameters of the dynamic model. Therefore, the dynamic buoy model is obtained considering environmental disturbances such as wind and waves. The mathematical model and the control algorithms are simulated and compared in MATLAB/Simulink. The comparison is made considering the presence of environmental disturbances from waves and wind. In addition, the evaluation was carried out using performance indicators such as variation in control efforts and those based on error: integral error, absolute integral error, and mean square error.

***Keywords*:** backstepping controller, marine systems, omnidirectional configuration, PD+ controller, vehicle dynamics

MSC: 37N35, 34A30, 70E60, 58E25, 70E60

Abbreviation

ASV	Autonomous Surface Vehicles
NEAT	Neuro-Evolution Algorithm of augmented Topologies
BOC	Buoys with Omnidirectional Configuration

Copyright ©2025 Yair Lozano-Hernández, et al.
DOI: https://doi.org/10.37256/cm.6220256208
This is an open-access article distributed under a CC BY license
(Creative Commons Attribution 4.0 International License)
https://creativecommons.org/licenses/by/4.0/

RBCD	Robust Backstepping Control ased on Data
DSMC	Data-based Sliding-Mode Control
SMC	Sliding Mode Control
PD+	Proportional-Derivative-Plus
IE	Integral Error
IAE	Integral of the Absolute Error
ASE	Average Square Error
TVCE	Total Variations of Control Efforts

Nomenclature

$\{n\}$	Inertial reference frame
o_n	Origin of intertial reference frame
x_n	x axis in intertial reference frame
y_n	y axis in intertial reference frame
z_n	z axis in intertial reference frame
$\{b\}$	Fixed coordinate system to the body
o_b	Origin of body-fixed reference frame
x_b	x axis in body-fixed reference frame
y_b	y axis in body-fixed reference frame
z_b	z axis in body-fixed reference frame
M_{CR_v}	Rigid body mass matrix
$C_{CR_v}(\nu)$	Rigid body Coriolis and centripetal matrix
m	Mass of the buoy
I_z	Moment of inertia of BOC
ν	Generalized speed vector expressed in $\{b\}$
u	Linear velocity in x direction
v	Linear velocity in y direction
r	Angular velocity about z axis
τ_{CR_v}	Generalized vector of external forces and moments expressed in $\{b\}$
τ_{wave}	Forces and time of waves
τ_{hid_v}	Hydrostatic forces and moment
τ_{windv}	Forces and time of wind
τ_v	Forces and time of control
M_{A_v}	Mass matrix generated by inertia the fluid surrounding the buoy
$C_{A_v}(\nu)$	Coriolis and centripetal matrix
D_v	Damping matrix
$X_u,\ Y_v,\ N_r$	Linear damping coefficients
$X_{\dot{u}},\ Y_{\dot{v}},\ N_{\dot{r}}$	Hydrodynamic added mass coefficients

1. Introduction

The maritime coasts have been monitored for navigation and coastal security reasons. However, the climatic changes of the last decades have had repercussions in several countries, including the safety of people living near the coasts [1]. To understand the impact of waves on oceanic and atmospheric models, it is crucial to understand dissolvedness and temperature. These data are essential for various research fields, including wave dynamics, air-sea coupling, gas exchange, remote acoustic detection and microwave, and water quality monitoring and marine ecosystems. However, it is important

to emphasize that the mobility of these systems is a critical factor that allows precise measurements at different locations of the ocean. In this sense, the flexibility to move from one point to another is a key feature in the selection of a monitoring system [2].

In recent decades, significant evolution has been seen in buoy technology used to monitor the marine environment. Modern buoys are increasingly autonomous and are equipped with integrated sensors that measure parameters such as temperature, salinity, water pressure, speed and wind direction. In addition, they have satellite communication systems that allow them to transmit data in real time to monitoring centers [3]. Mobile buoys, on the other hand, can move through water thanks to the use of propellants, allowing them to make measurements at different locations [4].

Regarding the study and use of Autonomous Surface Vehicles (hereinafter, ASV) for monitoring, [5] describes the design of an environmental monitoring system in a large region with a reduced number of ASVs. Optimal sampling strategies are developed considering the quality of the estimated environmental field and the useful life of the sensors. Also, experimental results of temperature monitoring in an outdoor swimming pool using an ASV are presented.

In [6] decentralized control is proposed in a set of aquatic surface vehicles. Robots are controlled by an evolved neuronal network. For the evolution of neuronal networks, the Neuro-Evolution Algorithm of augmented Topologies (NEAT) is used and from the simulations and tests the best evolved controllers were taken to perform the complex tasks of initial position, dispersion, or grouping.

On the other hand, in [7] vehicles that are used have an omnidirectional mobile design, which allows them to take an arbitrary position or stay at a fixed point for a long period of time. To maintain low electricity consumption, the use of electronic components is limited, and the navigation system is composed of a Global Positioning System (GPS) and a six-axle sensor, each vehicle moves autonomously so there is no communication between vehicles.

In addition, in [8] Buoys with Omnidirectional Configuration (hereinafter, BOC) are used. The propulsion arrangement consists of three separate capsules at 120° with two engines each. The behavior can be visualized as a state machine with three main stages: sensor reading, decision making and movement.

Regarding the control of marine vehicle actuators, [9] seek to determine the threshold for the computational rate needed in controllers to accurately follow discontinuous square wave commands required for Unmanned Surface Vehicle (USV) actuators; to do so, they use discrete Deterministic Artificial Intelligence (DAI), and all approaches are validated in MATLAB simulations. On the other hand, in [10], learning and adaptation techniques are implemented to control DC motors used to drive the control of a USV; the controller design allows it to adapt based on variations or uncertainty of the system parameters.

In addition to the design of a control algorithm, [11] presents a new approach of Robust Backstepping Control based on Data (RBCD) for monitoring ASV trajectory with uncertainties and unknown dynamics parameters. The proposed approach effectively integrates the backstepping decoupling technique and Data-based Sliding-Mode Control (DSMC). The approach also uses an extended state observer to compensate for unknown couplings and dynamics parameters. Experimental results in a prototype validate the effectiveness of the proposed RBCD approach.

In [12], an omnidirectional Unmanned Surface Vehicle (USV) with a magnet-based docking system is presented for construction tasks on water surfaces. Yin et al. designed an unmanned vessel (with overdrive), which is capable of moving omnidirectional [13].

In this type of vehicle, unpredictable wave disturbances are the main factor directly affecting position drift and attitude stability. These disturbances can be compensated by two design features; a stable structure and a robust motion controller. Therefore, several path planning and tracking algorithms have been proposed that can be applied to water surfaces [14]; however, they do not consider the effect of waves on the robot's displacement.

There are several works focused on the design of control strategies for ASVs, such as: PID control; adaptive control; sliding mode control [15]; Model Predictive Control (MPC); cascade control, etc.

Casavola et al. worked on motion coordination for a set of omnidirectional USVs, which are dynamically decoupled and subject to local obstacle constraints; to achieve this, they use a supervision scheme based on a Distributed Command Governor [16]. In [17] the design of a heading controller based on the use of a fuzzy sliding mode is reported, fuzzy algorithms are used to optimize the sliding mode control, thus improving the stability and robustness of the controller. On

the other hand, according to what was reported in [18], given the non-linearity of USVs, it is possible to apply real-time Non-linear Model Predictive Control (NMPC) schemes for trajectory tracking tasks.

In work [19], a learning control method is presented by reinforcement of the model reference for uncertain ASV. The proposal combines a model-based control method with deep reinforcement learning. A nominal system for the design of the reference control law is used using a conventional control approach. The proposal provides guarantees of stability and better sampling efficiency compared to traditional learning methods for deep reinforcement.

Besides, [20] present the deterministic artificial intelligence applies to the heading control of an submarine (Rov) vehicle simulated remotely. The authors integrate the used code, also illustrate the autonomous control of a vehicle remotely operated VLBV 300 in the first step of a shaped square wave command, and the error decreased an additional sixty -two percent Square Wave Command step.

Similarly in [21], they propose adaptive and learning methods and are compared with the control of DC engines that act as control surfaces of unmanned submarine vehicles. The adaptation methods included are the model Fliguar method is based on the algebraic design, and is analyzed together with parameter estimation methods, as minimum recursive square, extended square minimums and minimum squares by lots. Also, they simulate the artificial intelligence of monitoring of the model and deterministic, and the respective performance metrics are evaluated and compared for transitory response and input monitoring. In this, the deterministic artificial intelligence that worked exceeded the modeling approach in a minimum maximum transitory value in a percentage range of approximately 2 to 70%, but the model control achieved at least 29% less error in the entry control than the deterministic artificial intelligence.

On the other hand, [22] presents a Sliding Mode Control scheme (hereinafter, SMC) activated by events to track asvs. The proposal of the SMC scheme with events guarantees the precision of the control and the low-frequency actions of the actuator, reducing both the wear and the energy consumption of the actuators, compared to the controller with a traditional time shot. The proposed controller not only guarantees a bounded steady-state error but also guarantees the non-accumulation of intermediate execution times.

To obtain a set of BOCs that work in a coordinated and efficient manner, it is necessary to design control schemes that guarantee compliance with the control objective, such as tracking trajectories from one point to another. The control algorithms used must be robust to the adversities of the environment in which they are located and at the same time, guarantee correct compliance with the control objective.

The design of control schemes for these systems is an interesting problem, since its dynamic is complex, non-linear and sensitive to exogenous disturbances. In addition, the environment in which the buoy operates is extremely variable and can be difficult to model and predict. Therefore, the design of efficient and robust control schemes is crucial to guarantee a precise and stable displacement of the buoy in its environment. From the above, the need to develop control schemes for autonomous buoys capable of moving from one point to another is highlighted.

For this work, the use of the BOC is considered to have unique advantages in making strong turns and allowing the buoy to be deep; monitoring of marine objectives; autonomous navigation on turbulent surfaces; inter alia. In addition, two control schemes based on the non-linear dynamic model of the BOCs are designed for trajectory monitoring. The simulation is performed in the presence of disturbances to analyze the performance of the control schemes.

1.1 *Problem statement and organization of work*

The objective of this work is to derive the mathematical model of a BOC considering disturbances due to waves and wind gusts. Then, to propose control algorithms to move the BOC from one reference point to another within the X, Y plane despite the presence of disturbances. For this, two feedforward control schemes are proposed in combination with: (1) Proportional Derivative Plus controller; and (2) Backstepping controller. Both control schemes consider: the complex, non-linear dynamics and sensitivity to exogenous disturbances of the BOC; the use of the mathematical model for its design; access to all system variables; and a Lyapunov stability analysis for its deduction.

The organization of this work is as follows. Section 2 describes the work directly related to the proposal developed in this research. Section 3 describes the fundamental equations of the BOC dynamic model, considering disturbances due to wind and waves; Also, the operating dynamics of the omnidirectional configuration is described. Section 4 presents the

design of the proposed control schemes. Section 5 shows numerical tests and results of control schemes under different disturbance inputs. Finally, the conclusions of the work and some future works are given.

2. Related works

Fujii et al. presented a design for a monitoring device for aquatic environments. The device is an omnidirectional robot with a low manufacturing cost and sustainable operation. The sensor device consists of four actuators placed in a cross shape, which allows it to move to a reference point and perform in situ monitoring of water environmental data. Additionally, they developed a control strategy to keep their robot in a desired position, which was numerically simulated and physically implemented. Their strategy focuses on a distributed predictive control scheme [23].

As a continuation of the previous proposal, Fujii et al. also worked on strategies to regulate the position and prolong the energy duration of the omnidirectional robot (with symmetrical shape) for in-situ monitoring. They simulated and implemented optimal position-keeping strategies considering the effects of disturbances. In this study, the robot was controlled using the PD controller, and the distance between the robot position and the target position determined the thrust power [24].

Xue et al. developed a low-cost omnidirectional robotic platform. The robot has an isotropic cylindrical body design and its motion is due to its omnidirectional configuration, which consists of 3 propellers [25]. They implemented a model predictive controller for motion control, this controller allowed them to decouple the multiple inputs and outputs, and they even comment that the tuning was simpler compared to that of a traditional PID.

As mentioned in previous works, symmetric designs in aquatic robots allow them to move efficiently in all directions. Moreover, the robot can maintain its position even in the presence of disturbances (for more information on surface robots with symmetric shapes, see [26, 27]). Regarding the omnidirectional propulsion configuration, it allows for agile movements, as well as better compensation for the rapid variation of drag and damping when switching between wave and roll directions.

It is important to highlight that unlike the propulsion system proposed by Xue et al., in this work 6 actuators (3 pairs) are considered, which is due to the fact that brushless motors (without the possibility of reversing rotation) are planned to be used in its future implementation. The decision to use this configuration is based on the existence of non-holonomic restrictions with conventional two-propeller propulsion designs, as well as the consideration of using few actuators for movement in the X, Y plane; some other works that use other omnidirectional configurations are [8, 28].

In the control part, the control schemes proposed in this work consider the complex, non-linear dynamics and the sensitivity to exogenous disturbances of the BOC. In addition, both controllers arise from a Lyapunov stability analysis, guaranteeing asymptotic stability. It is important to highlight the use of indices based on error and control actions to analyze the advantages and disadvantages of the developed schemes, this being another of the differentiators compared to the works mentioned in this section.

Regarding the mathematical model, both Xue et al. and Fujii et al. show a dynamic model of their proposals; however, they do not address in detail the disturbances associated with waves and wind. In addition, they do not describe in detail the methodology they followed to obtain it. Another difference with these works is that they show only the value of the control actions, but not the calculation used to know the torque of each of the motors.

3. Derivation of BOC mathematical modeling

The mathematical modeling of BOC, as with any other marine vehicle, requires studying both static and dynamic aspects. The equilibrium of the body at rest or at constant velocity pertains to the static analysis, while the body with acceleration pertains to the dynamic analysis. From the rigid-body kinematics of a body maneuvering in a liquid environment, the study continues with the analysis of hydrodynamic and hydrostatic forces, followed by the breakdown and study of external forces due to wind and waves that affect the performance of the marine vehicle. Finally, the model is obtained in the global reference frame.

The mathematical model of a marine vehicle is expressed in terms of linear and angular velocities; therefore, its development is described in the fixed coordinate system to the body $\{n\} = (x_n,\ y_n,\ z_n)$ with origin (o_n) [29].

Figure 1a shows the upper view of the buoy with three bidirectional propellers positioned at 120° between each. The coordinates (x_b) and (y_b) represent the fixed position of the buoy within the fixed reference system associated with the body $\{b\} = (x_b, y_b, z_b)$. This reference system has its origin at (o_b). The propellants 1 and 2 are symmetrically aligned with the y_b axis and separated by an angle $\delta = 30°$ compared to the x_b axis. For this work, the BOC is considered to have three degrees of freedom, displacement on the X, Y axes and rotation on the Z axis (ψ angle).

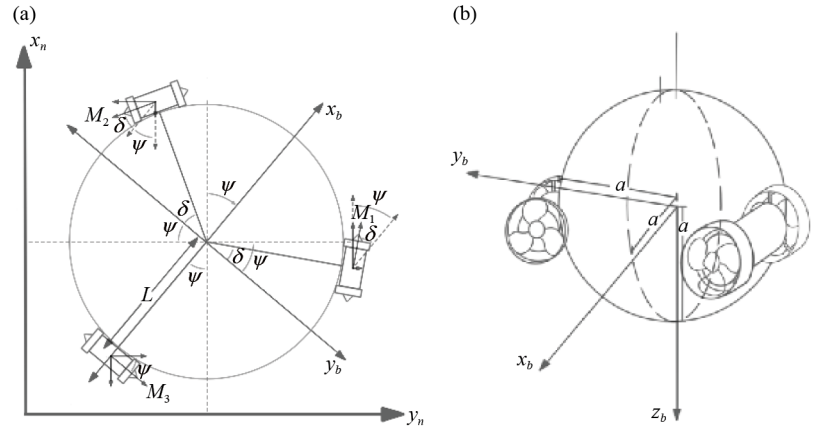

Projection of the axes per upper view of the BOC

Boya semi-axes

Figure 1. Axis projection

Control design requires equations of motion, which for rigid body dynamics can be derived by applying the Newtonian and Lagrangian formalism, which produce equations representing the translational and rotational motions. These equations can be expressed in a more compact form as [30]:

$$M_{CR_v}\dot{\nu} + C_{CR_v}(\nu)\nu = \tau_{CR_v}, \tag{1}$$

where, M_{CR_v} is the rigid body inertia matrix, $C_{CR_v}(\nu)$ is the coriolis matrix and the rigid centripetal body due to rotation of the framework $\{b\}$ compared to the inertial reference framework $\{n\}$. These are expressed as follows.

$$M_{CR_v} = \begin{bmatrix} m & 0 & 0 \\ 0 & m & 0 \\ 0 & 0 & I_z \end{bmatrix}, \tag{2}$$

$$C_{CR_v}(\nu) = \begin{bmatrix} 0 & 0 & -mv \\ 0 & 0 & mu \\ mv & -mu & 0 \end{bmatrix}, \tag{3}$$

with, m is the mass of the buoy, I_z is the moment of inertia of BOC, $\nu = [u,\ v,\ r]^T$ is the generalized speed vector expressed in $\{b\}$ and $\tau_{CR_v} = [X_v,\ Y_v,\ N_v]^T$ is the generalized vector of external forces and moments expressed in $\{b\}$.

In addition, external forces and moments are expressed as:

$$\tau_{CR_v} = \tau_{hid_v} + \tau_{hs_v} + \tau_{windv} + \tau_{wave_v} + \tau_v, \tag{4}$$

where,

$$\tau_{hid_v} = -M_{A_v}\dot{v} - C_{A_v}(v)v - D_v v,$$

$$\tau_{hs_v} = -g_v(\eta) - g_{o_v}, \tag{5}$$

in which, τ_{wave}, are forces and time of waves and must be expressed by the behavior of the wave that you want to represent on the 3 axes, τ_{hid_v} are hydrodynamic forces and moment, τ_{hs_v} are hydrostatic forces and moment, in this case, $\tau_{hs_v} = 0$ in the horizontal plane because balance and pitch are omitted [31]. τ_{windv} are forces and wind time, τ_v are forces and control time.

On the other hand, M_{A_v} is the matrix of added mass generated by inertia of the fluid surrounding the buoy, while $C_{A_v}(v)$ is the matrix of coriolis and centripetal, which is based on the added mass and is due to rotation of the frame of reference $\{b\}$ compared to $\{n\}$. The energy transported by waves generated on the surface as well as the friction of the buoy with the water, the cushioning for waves and the detachment of vortices generate the damping matrix D_v and it is usually approximate to its diagonal terms [30, 31]. These matrices are defined as follows.

$$M_{A_v} = -\begin{bmatrix} X_{\dot{u}} & 0 & 0 \\ 0 & Y_{\dot{v}} & 0 \\ 0 & 0 & N_{\dot{r}} \end{bmatrix}, \tag{6}$$

$$C_{A_v}(v) = \begin{bmatrix} 0 & 0 & Y_{\dot{v}}v \\ 0 & 0 & -X_{\dot{u}}u \\ -Y_{\dot{v}}v & X_{\dot{u}}u & 0 \end{bmatrix}, \tag{7}$$

$$D_v = -\begin{bmatrix} X_u & 0 & 0 \\ 0 & Y_v & Y_r \\ 0 & N_v & N_r \end{bmatrix}, \tag{8}$$

where the constants $X_{\dot{u}}$, $Y_{\dot{v}}$, $Y_{\dot{r}}$ and $N_{\dot{r}}$. X_u, Y_v, Y_r, N_v and N_r are hydrodynamic derivatives. For the particular case of a vessel in the form of a sphere 0 [32].

From the above, the components of the added mass are defined as [33, 34]:

$$X_{\dot{u}} = \frac{2}{3}\pi\rho a^3,$$

$$Y_{\dot{v}} = \frac{2}{3}\pi\rho a^3,$$

$$N_{\dot{r}} = 0, \tag{9}$$

a is the radius of the sphere. Hydrodynamic derivatives are defined as:

$$X_u = -\frac{8\pi\zeta_u[m + X_{\dot{u}}]}{T_{n,\ u}},$$

$$Y_v = -\frac{8\pi\zeta_v[m + Y_{\dot{v}}]}{T_{n,\ v}},$$

$$N_r = -\frac{8\pi\zeta_r[I_z + N_{\dot{r}}]}{T_{n,\ r}},$$

$$T_i = -\frac{T_{n,\ i}}{8\pi\zeta}, \tag{10}$$

where, ζ_i is the relative damping coefficient and T_i is a constant of time with typical values of 100-250s with $i = u,\ v,\ r$.

Furthermore, the constants V_w and γ_w correspond to the wind speed and the angle of attack, respectively (see Figure 2a):

$$\tau_{wind_v} = \frac{1}{2}\rho_a V_w^2 \begin{bmatrix} C_X(\gamma_w)A_{F_w} \\ C_Y(\gamma_w)A_{L_w} \\ C_N(\gamma_w)A_{L_w}L_{oa} \end{bmatrix}, \tag{11}$$

where, ρ_a is air density, $C_i(\gamma_w)$ are current coefficients depending on the angle of attack with $i = X,\ Y,\ N$. A_{F_w} is the projected frontal area, A_{L_w} is the projected lateral area, L_{oa} is the length of the buoy. For each of the degrees of freedom, current coefficients are expressed as:

$$C_X(\gamma_w) = -C_{X,\ max} * \cos(\gamma_w) * |\cos(\gamma_w)|,$$

$$C_Y(\gamma_w) = C_{Y,\ max} * \sin(\gamma_w) * |\sin(\gamma_w)|,$$

$$C_N(\gamma_w) = C_{N,\ max} * \sin(2 * \gamma_w). \tag{12}$$

The generalized induced forces τ_v must be represented with respect to the thrust of the engines and within the framework of fixed reference to the buoy $\{b\}$ [35].

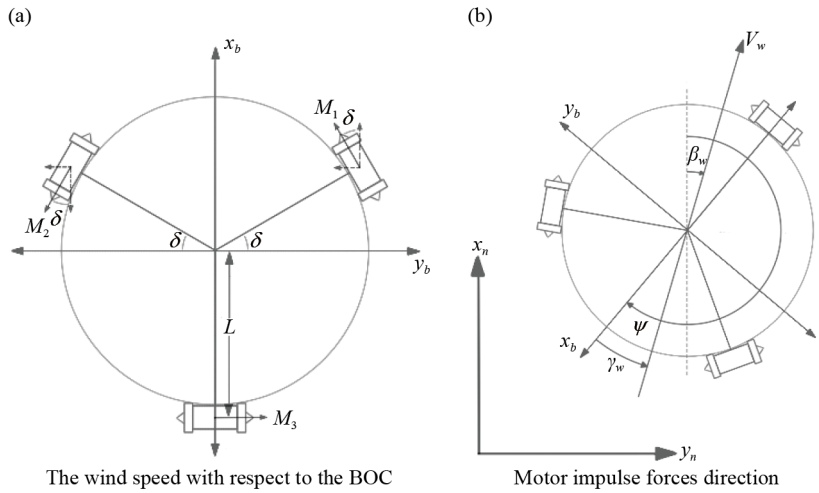

Figure 2. Direction of the component of the speed and impulse of the engines

$$\tau_v = B_v \tau_{prop}, \tag{13}$$

where,

$$B_v = \begin{bmatrix} \cos\delta & -\cos\delta & 0 \\ -\sin\delta & -\sin\delta & 1 \\ L & L & L \end{bmatrix}, \tag{14}$$

$$\tau_{prop} = \begin{bmatrix} M_1 \\ M_2 \\ M_3 \end{bmatrix}. \tag{15}$$

Subsequently, the dynamics of the BOC can be represented when (4) is replaced with (1)

$$M_v \dot{v} + C_v(v)v + D_v(v)v = \tau_v + \tau_{wind_v} + \tau_{wave_v}, \tag{16}$$

where

$$\begin{aligned} M_v &= M_{A_v} + M_{CR_v}, \\ C_v(v_r) &= C_A(v_r) + C_{CR}(v_r). \end{aligned} \tag{17}$$

Then, the model in (16) is expressed in the frame of reference $\{b\}$. Therefore, to obtain the model in the global coordinate system $\{n\}$, which expresses the position of the BOC, the transformation $\nu = R_n^b \dot{\eta}$ is proposed, then [36]:

$$\dot{\nu} = R_n^b \ddot{\eta} + \dot{R}_n^b \dot{\eta}, \tag{18}$$

where, R_n^b is the transformation matrix of $\{n\}$ to $\{b\}$, $\eta = [x,\ y,\ \psi]^T$

$$R_n^b = \begin{bmatrix} \cos\psi & \sin\psi & 0 \\ -\sin\psi & \cos\psi & 0 \\ 0 & 0 & 1 \end{bmatrix}. \tag{19}$$

Replacing (18) into (16), and multiplying everything by $R_b^n = (R_n^b)^{-1}$, the mathematical model is obtained within the global reference frame expressed as:

$$R_b^n M_\nu (R_n^b \ddot{\eta} + \dot{R}_n^b \dot{\eta}) + R_b^n C_\nu(\nu) R_n^b \dot{\eta} + R_b^n D_\nu(\nu) R_n^b \dot{\eta} = R_b^n \tau_\nu + R_b^n \tau_{wind_\nu} + R_b^n \tau_{wave_\nu}. \tag{20}$$

Finally, it is simplified (20) to obtain the position equations following:

$$M\ddot{\eta} + C(\eta,\ \dot{\eta})\dot{\eta} + D(\eta)\dot{\eta} = B\tau + \tau_w, \tag{21}$$

with

$$\begin{aligned} M &= R_b^n M_\nu R_n^b, \\ C(\eta,\ \dot{\eta}) &= \left[R_b^n M_\nu \dot{R}_n^b + R_b^n C_\nu(\nu) R_n^b \right], \\ D(\eta) &= R_b^n D_\nu(\nu) R_n^b, \\ \tau &= \tau_{prop}, \\ B &= R_b^n B_\nu, \\ \tau_w &= R_b^n \tau_{wind} + R_b^n \tau_{wave}. \end{aligned} \tag{22}$$

In complement to the above, the physical parameters of the system required by modeling are shown in Table 1.

Table 1. BOC parameters

Parameter	Notation	Value
Mass	m	9.5 kg
BOC center length to the center of the propeller	L	0.175 m
Boya radio	a	0.17 m
Moment of inertia about z	I_z	0.0207 $kg \cdot m^2$
Derived mass added in x	$X_{\dot{u}}$	8.801 kg
Derived mass added in y	$Y_{\dot{v}}$	8.801 kg
Derived mass added in ψ	$N_{\dot{r}}$	0 $kg \cdot m^2$
Hydrodynamic derivative in x	X_u	0.183 kg
Hydrodynamic derivative in y	Y_v	0.183 kg
Hydrodynamic derivative in ψ	N_r	0 $kg \cdot m^2$

4. Design of control schemes

The BOC system has three variables to control, the position on the translation axes (x, y) and the orientation in the rotation axis (ψ). The three coordinates are used in the system, which can be controlled directly.

4.1 *PD+ controller*

A Proportional-Derivative-Plus (PD+) controller is proposed. Furthermore, considering the success of using quadratic-type Lyapunov functions for stability study in interconnected systems, as well as its effectiveness in demonstrating asymptotic stability [37]. Considering (21), the following candidate Lyapunov function is proposed:

$$V(t) = \frac{1}{2}(\dot{e}^T M \dot{e} + e^T K_P e). \tag{23}$$

The above equation is proposed considering that, under soft conditions, any weighted sum of quadratic-type Lyapunov functions for reduced and boundary-layer systems is a quadratic-type Lyapunov function for the singularly perturbed system when the perturbation parameter is sufficiently small [38]. K_P is a positive symmetric matrix as

$$K_D = \begin{bmatrix} K_{D_x} & 0 & 0 \\ 0 & K_{D_y} & 0 \\ 0 & 0 & K_{D_\psi} \end{bmatrix}, \tag{24}$$

and the monitoring error e is defined as:

$$e(t) = \eta(t) - \eta^*(t), \tag{25}$$

being, η the position vector and η^* the desired position vector. Then, when deriving (23) with respect to time, we obtain:

$$\dot{V}(t) = \dot{e}^T M\ddot{e} + \frac{1}{2}\dot{e}^T \dot{M}\dot{e} + \dot{e}^T K_P e, \tag{26}$$

in addition, equation (21) can be rewritten as:

$$M\ddot{e} = B\tau + \tau_w - C(\eta,\ \dot{\eta})\dot{\eta} - D(\eta)\dot{\eta} - M\ddot{\eta}^*, \tag{27}$$

moreover, $C(\eta,\ \dot{\eta})\dot{\eta}$ can be written as $C(\eta,\ \dot{\eta})\dot{\eta} = C(\eta,\ \dot{\eta})\,(\dot{e} + \dot{\eta}^*)$, then, replacing (27) with (26) is obtained:

$$\dot{V}(t) = \dot{e}^T\left[B\tau + \tau_w - C\,(\eta,\ \dot{\eta})\,(\dot{e} + \dot{\eta}^*)\ - D(\eta)\dot{\eta} - M\ddot{\eta}^*\right] + \frac{1}{2}\dot{e}^T \dot{M}\dot{e} + \dot{e}^T K_P e,$$

$$\dot{V}(t) = \dot{e}^T\left[B\tau + \tau_w - C\,(\eta,\ \dot{\eta})\,\dot{\eta}^* - D(\eta)\dot{\eta} - M\ddot{\eta}^*\ + K_P e\right] + \frac{1}{2}\dot{e}^T\left(\dot{M} + 2C\,(\eta,\ \dot{\eta})\right)\dot{e}, \tag{28}$$

taking advantage of the property where $\dot{M} + 2C\,(\eta,\ \dot{\eta})$ results in a symmetric skew matrix S and defining the controller $B\tau$ of the form:

$$B\tau = D(\eta)\dot{\eta} + C\,(\eta,\ \dot{\eta})\,\dot{\eta}^* - \tau_w + M\ddot{\eta}^* - K_P e - K_D\dot{e}, \tag{29}$$

where, K_D is a positive symmetric matrix as

$$K_D = \begin{bmatrix} K_{D_x} & 0 & 0 \\ 0 & K_{D_y} & 0 \\ 0 & 0 & K_{D_\psi} \end{bmatrix}, \tag{30}$$

after this, the (28) equation can be rewritten as

$$\dot{V}(t) = -\dot{e}^T K_D\dot{e}. \tag{31}$$

Thus, $\dot{V} \leq 0$, guarantees the stability of the system that the dynamics of error tends to zero in a finite time t_1. Thus, the selection of profits must ensure that the characteristic polynomial is Hurwitz [39], so the following reference model is used

$$s^2 + 2\zeta_i\omega_{n_i}s + \omega_{n_i}^2 = s^2 + K_D s + K_P. \tag{32}$$

In this way, $K_P = \omega_{n_i}^2$ and $K_D = 2\zeta_i\omega_{n_i}$. Figure 3 presents the schematic of the proposed PD+ controller.

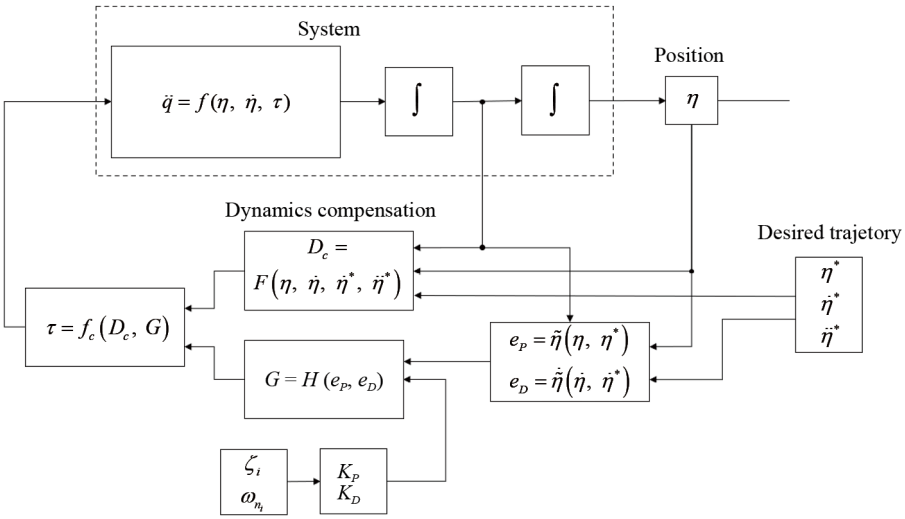

Figure 3. PD+ controller scheme

Finally, Table 2 shows the controller gains K_P and K_D used during the simulations.

Table 2. Gain values for PD+ controller

Gain	Value
K_{P_x}	94.1
K_{P_y}	94.1
K_{P_ψ}	3.24
K_{D_x}	87.3
K_{D_y}	87.3
K_{D_ψ}	3.96

4.2 *Backstepping controller*

For the design of this controller, it is based on the BOC model described in (21). The system is rewritten in the form of states space such as:

$$\xi_1 = \eta,$$

$$\xi_2 = \dot{\xi}_1 = \dot{\eta},$$

$$\dot{\xi}_2 = \ddot{\eta}, \tag{33}$$

where, $\xi_i = [\,\xi_{i_x}\ \xi_{i_y}\ \xi_{i_\psi}\,]^T$ with $i = 1,\ 2$. Therefore, the monitoring error is

$$z_1 = \xi_1^* - \xi_1, \tag{34}$$

with, $z_1 = [z_{1_x}\, z_{1_y}\, z_{1_\psi}]^T$ y ξ_1^* is the desired trajectory.

Subsequently, a Lyapunov candidate function is proposed under error

$$V(z_1) = \frac{1}{2} z_1^T z_1,$$

$$\dot{V}(z_1) = z_1(\dot{\xi}_1^* - \xi_2). \tag{35}$$

According to the Lyapunov stability theorem, (35) must be negative semidefinite, therefore the following equality must be satisfied

$$\dot{V}(z_1) \leq -\alpha_1 z_1^T z_1, \tag{36}$$

with α_1 equal to:

$$\alpha_i = \begin{bmatrix} \alpha_{i_x} & 0 & 0 \\ 0 & \alpha_{i_y} & 0 \\ 0 & 0 & \alpha_{i_\psi} \end{bmatrix}, \tag{37}$$

$\alpha_{i_j} > 0$; width $i = 1,\ 2;\ j = x,\ y,\ \phi$. Then, combining (36) and (35), results in

$$\xi_2 = \dot{\xi}_1^* + \alpha_1 z_1. \tag{38}$$

For the next step, a variable change is necessary for Z_2, therefore, it is defined as $z_2 = \xi_2 - \dot{\xi}_1^* - \alpha_1 z_1$ [40]. Then, the following increased Lyapunov function is proposed

$$V(z_1,\ z_2) = \frac{1}{2} z_1^T z_1 + \frac{1}{2} z_2^T z_2,$$

$$\dot{V}(z_1,\ z_2) = z_1^T \dot{z}_1 + z_2^T \dot{z}_2. \tag{39}$$

Using the same criteria as used in (35), (39) must satisfy

$$\dot{V}(z_1,\ z_2) \leq -\alpha_1 z_1^T z_1 - \alpha_2 z_2^T z_2. \tag{40}$$

From the definition of $\dot{\xi}_2 = \ddot{\eta}$ y (40), result

$$\ddot{\eta} = -\alpha_2 z_2 + z_1 + \ddot{\xi}_1^* - \alpha_1 z_2 - \alpha_1^2 z_1. \tag{41}$$

Finally, replacing (41) in (21), the following control law is obtained

$$B\tau = M(-\alpha_2 z_2 + z_1 + \ddot{\xi}_1^* - \alpha_1 z_2 - \alpha_1^2 z_1) + C(\eta,\ \dot{\eta})\dot{\eta} + D(\eta)\dot{\eta} - \tau_w. \tag{42}$$

In Figure 4 the backstepping control scheme is shown. It can be seen that the PD+ control scheme (Figure 3) is similar, because the two controls share several characteristics.

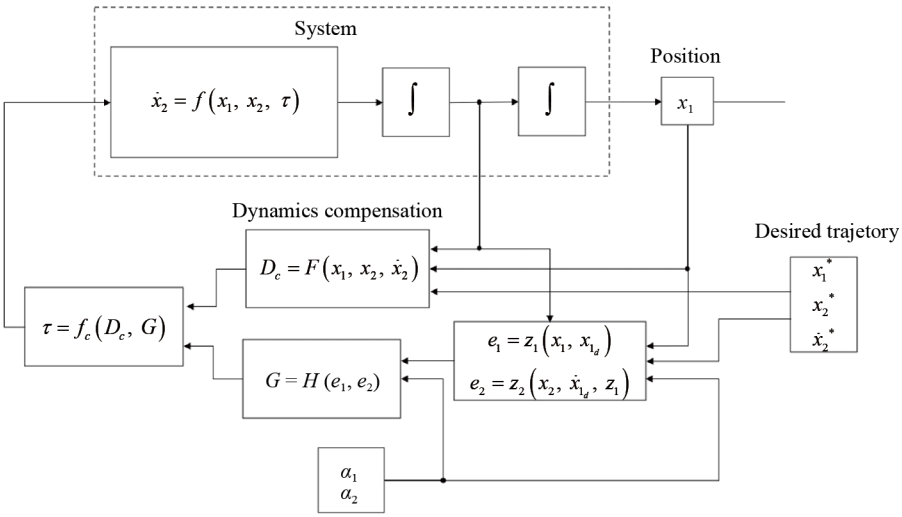

Figure 4. Backstepping controller scheme

From the above, the proposed profits for the controller are described in Table 3.

Table 3. Gains values for backstepping controller

Gains	Value
α_{1_x}	18
α_{1_y}	18
α_{1_ψ}	22
α_{2_x}	15
α_{2_y}	15
α_{2_ψ}	12

5. Simulation

To perform calculations corresponding to obtaining the mathematical model, as well as to experiment with the behavior of the translation and rotation variables x, y, ψ of the system, only MATLAB software and basic Simulink tools were used. In the first experiment, an environment was considered without environmental forces and moments, and in the second experiment the parameters previously defined for environmental forces and moments were used. It is essential to note that although the controller design is capable of handling the feedback of environmental disturbances, these disturbances are not feedback to the controller because wave measurements will not be obtained in the physical application. The control parameters used are the same as mentioned in Tables 2 and 3.

For the external wind force, the parameters were taken based on [29] and are defined in Table 4. The proposed wind speed is $10\frac{m}{s}$, which is at number 5 on the Beaufort scale (fresh breeze, 10-28 km/h) [41]. The angle of attack changes following the equation of a slope, $\gamma_w = 0.2t$, this trajectory is designed to know the behavior of the buoy in scenarios in which it is required to reach desired reference points with a predefined orientation or even to perform maneuvers in which it is necessary to maneuver on the ψ axis.

Table 4. Wind parameters

Parameter	Notation	Value
Current coefficient in x	$C_{X,\,max}$	0.46
Current coefficient in y	$C_{Y,\,max}$	0.46
Current coefficient in N	$C_{N,\,max}$	0.01

The following sine functions arrangement is proposed to simulate the forces of the waves

$$\tau_{wave} = a_i * \sin(w_i * t + b_i), \tag{43}$$

for $i = X,\ Y,\ N$. The parameters for each of dregrees of freedom are defined in Table 5, these parameters correspond to the maximum values that both controllers can compensate, i.e. the maximum value of the permissible disturbances.

Table 5. Wave parameters

Parameter	Value
a_X	15
w_X	2
b_X	3
a_Y	15
w_Y	2
b_Y	3
a_N	1.5
w_N	1
b_N	1

5.1 *Results*

In the simulation, the PD+ control schemes and the backstepping are submitted to compare their yields before the metric of the integral of the quadratic error. Therefore, three cases of desired trajectory studies are generated under the same operating conditions and disturbances, these disturbances are described by τ_w.

The first shows a straight line movement that with an inclination of $\pi/2$ and that begins from a point of origin from 0 to 20 m for both coordinates. This trajectory is generated by tow Bezier polynomials for each axis, starts at 0 m and reaches a value of 20 m on the x and y axes in a start time of 5 s and reaching its maximum time at 45 s, while seeking to stabilize ψ at 0 rad. The second case shows a circle trajectory with its center at the origin of the XY plane and the radio 0.8 m. The equations for the trajectories for each coordinate for this case are described by:

$$x^* = 0.8\cos\left(\frac{\pi}{15}t\right),$$

$$y^* = 0.8\cos\left(\frac{\pi}{15}t\right),$$

$$\psi^* = 0.1t. \tag{44}$$

Finally, the third case shows a trajectory in the form of a clover for the XY plane that seeks to stabilize ψ in 0 rad. The equations for the trajectories for each coordinate for this case are described as

$$x^* = 3\sin(0.3t)\cos(0.1t),$$

$$y^* = 3\sin(0.3t)\sin(0.1t),$$

$$\psi^* = 0. \tag{45}$$

Figure 5 shows the desired path, the response by the PD+ controller and the backstepping (BS) of the three cases on the XY plane. These graphs show that both controls have oscillations around the paths of cases two and three.

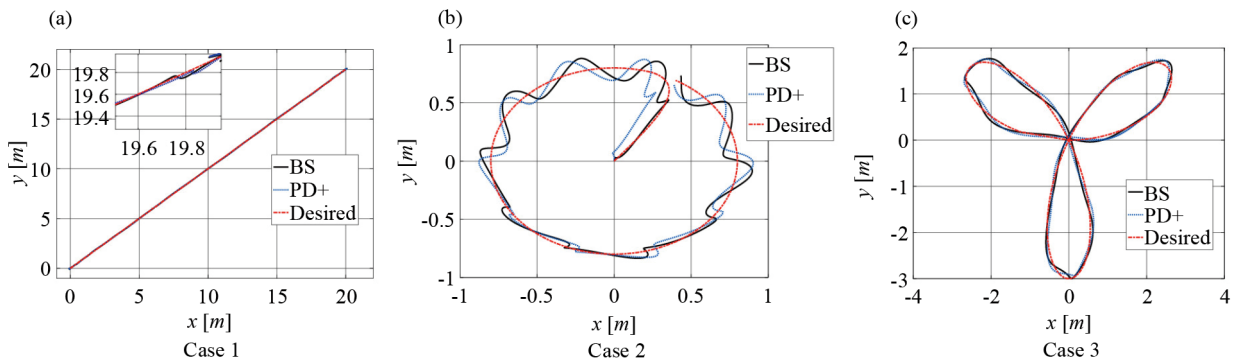

Figure 5. Responses obtained on the X, Y axes to the proposed control schemes

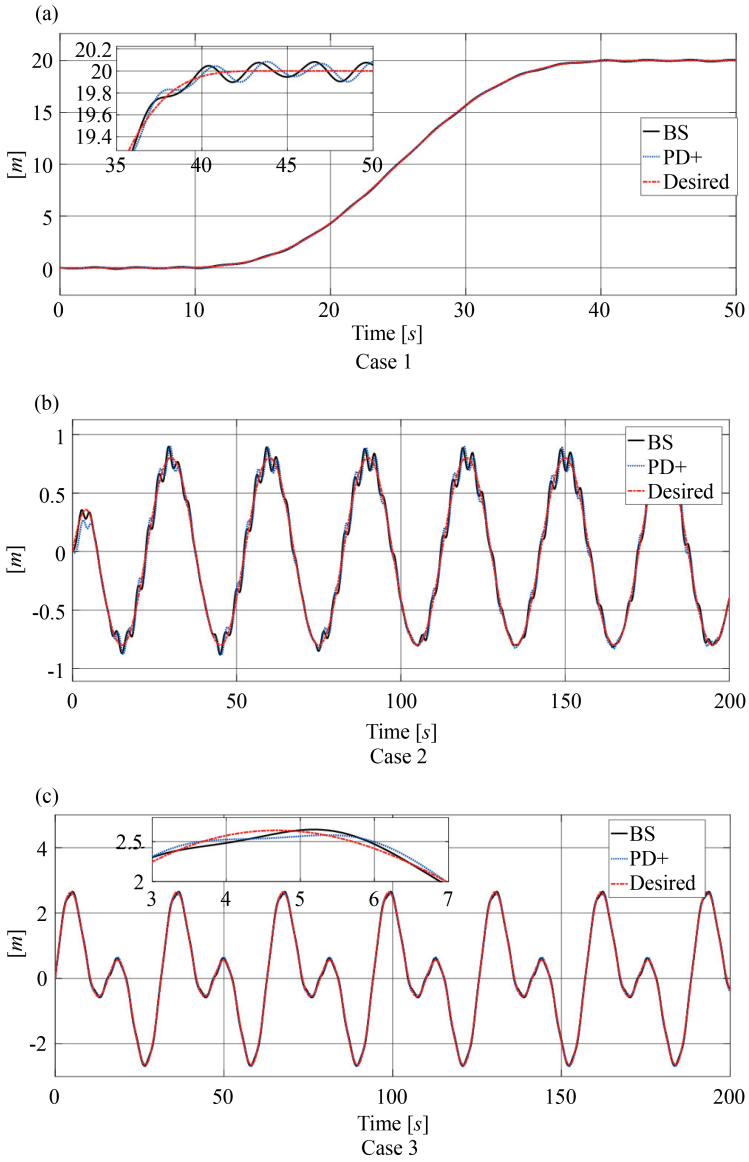

Figure 6. Responses obtained on the X axis due to the proposed control schemes

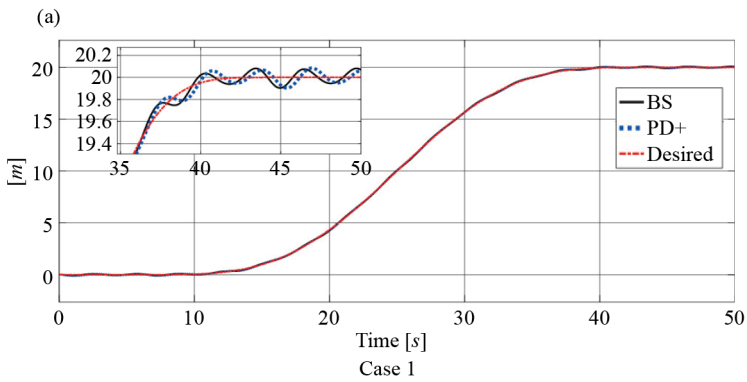

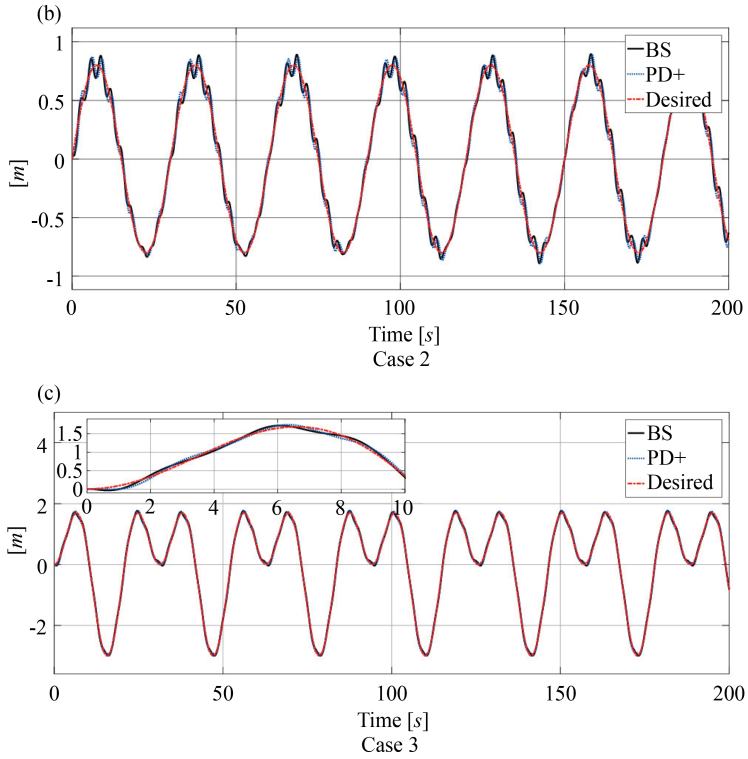

Figure 7. Responses on the Y axis due to the proposed control schemes

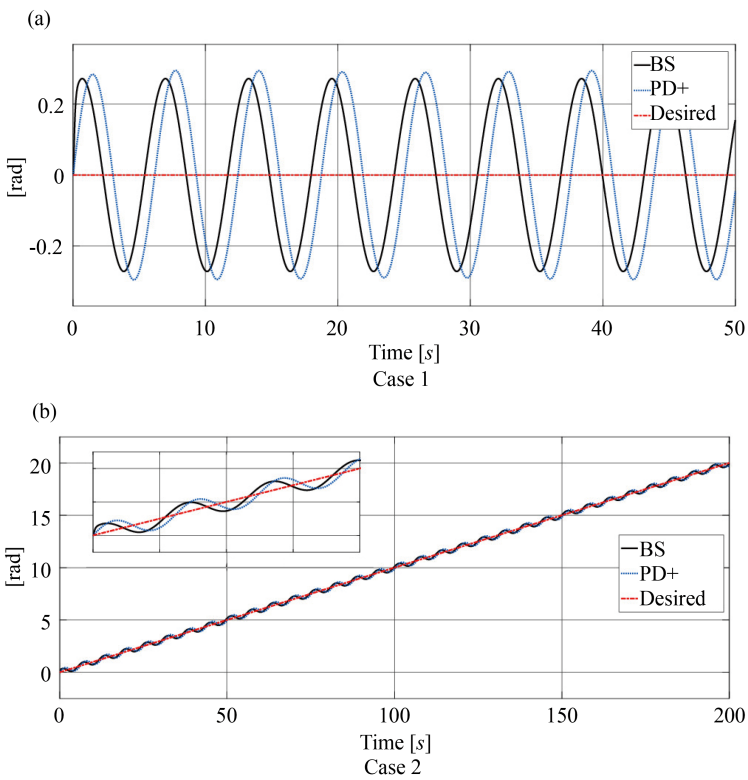

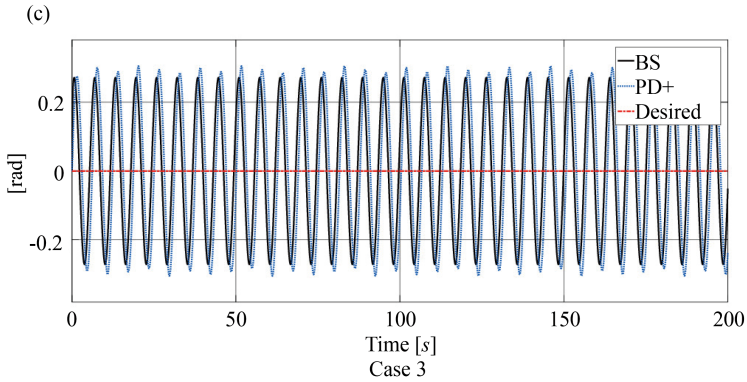

Figure 8. Responses on the ψ axis due to the proposed control schemes

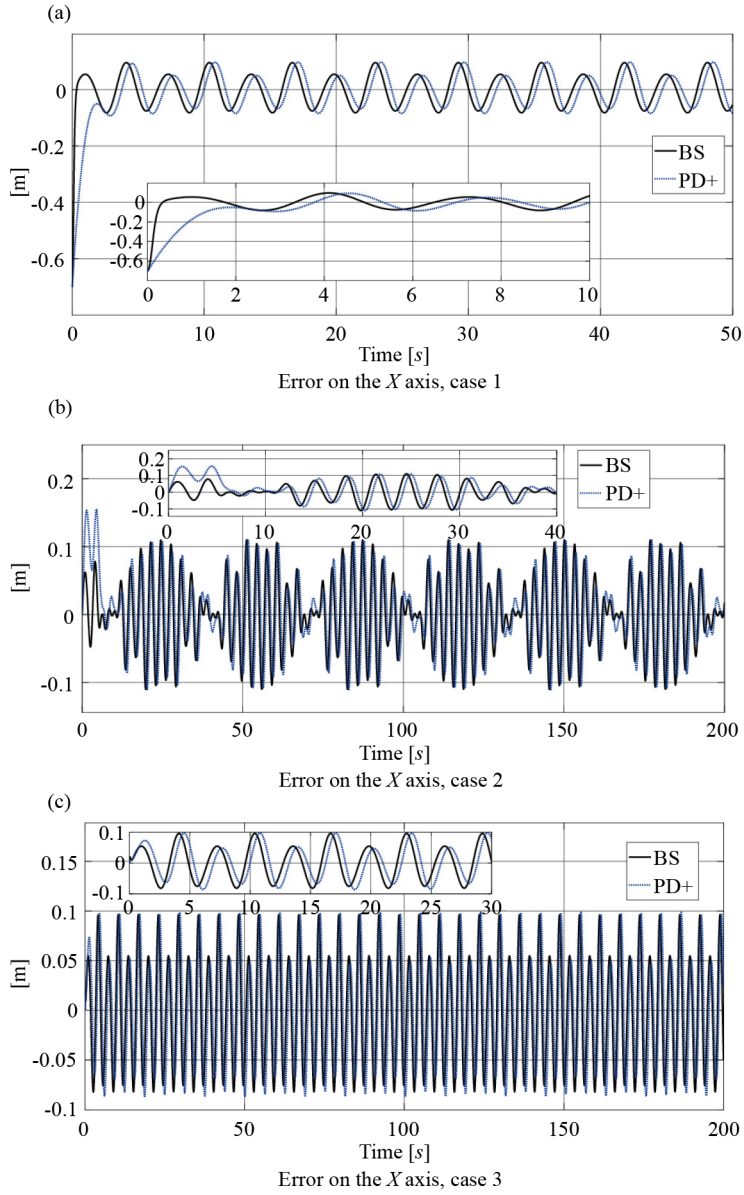

(d)

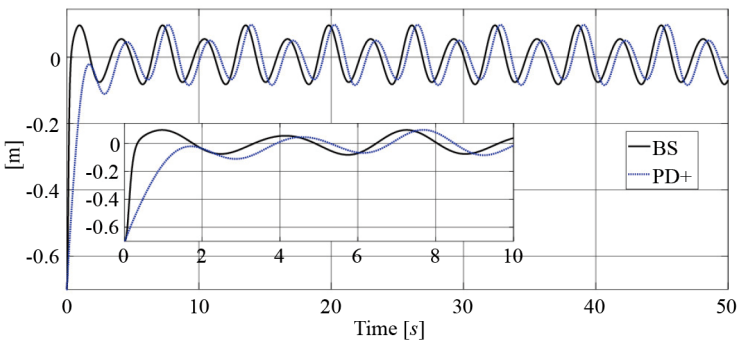

Error on the Y axis, case 1

(e)

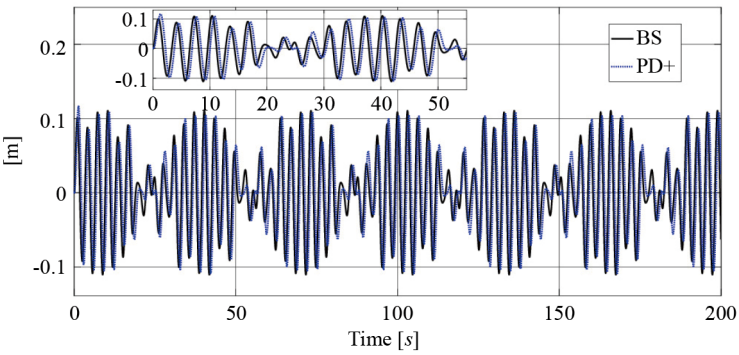

Error on the Y axis, case 2

(f)

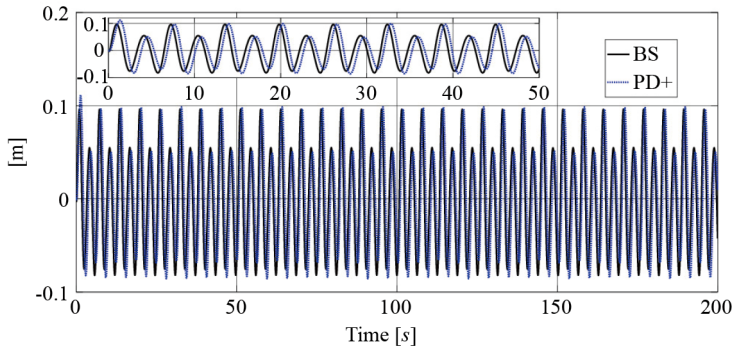

Error on the Y axis, case 3

(g)

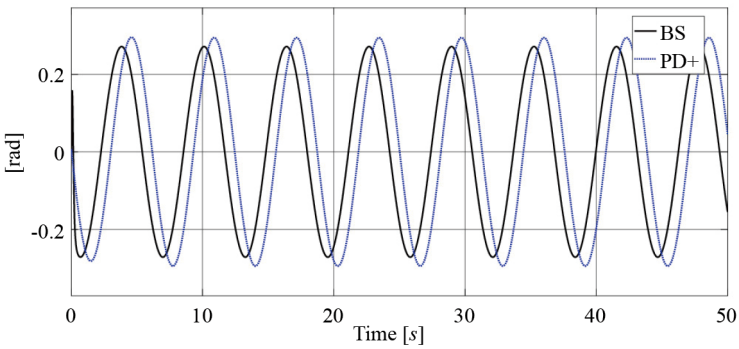

Error on the ϕ axis, case 1

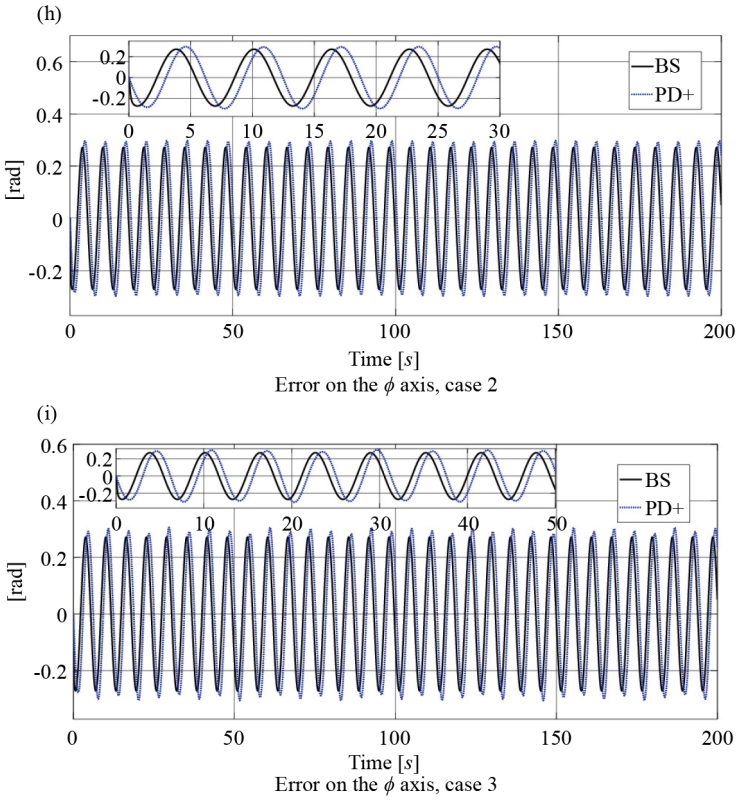

Figure 9. Error behavior on the X, Y and ψ axes

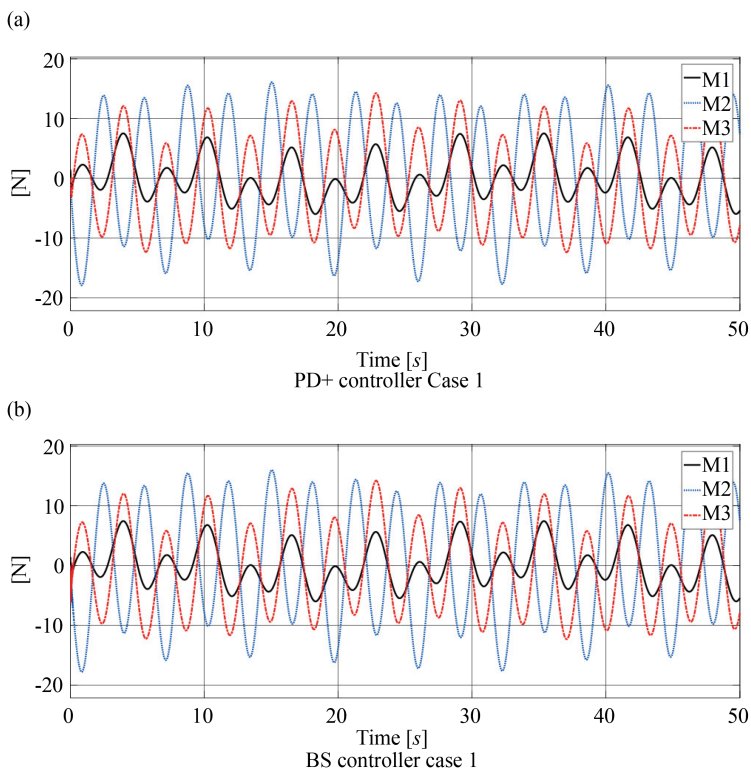

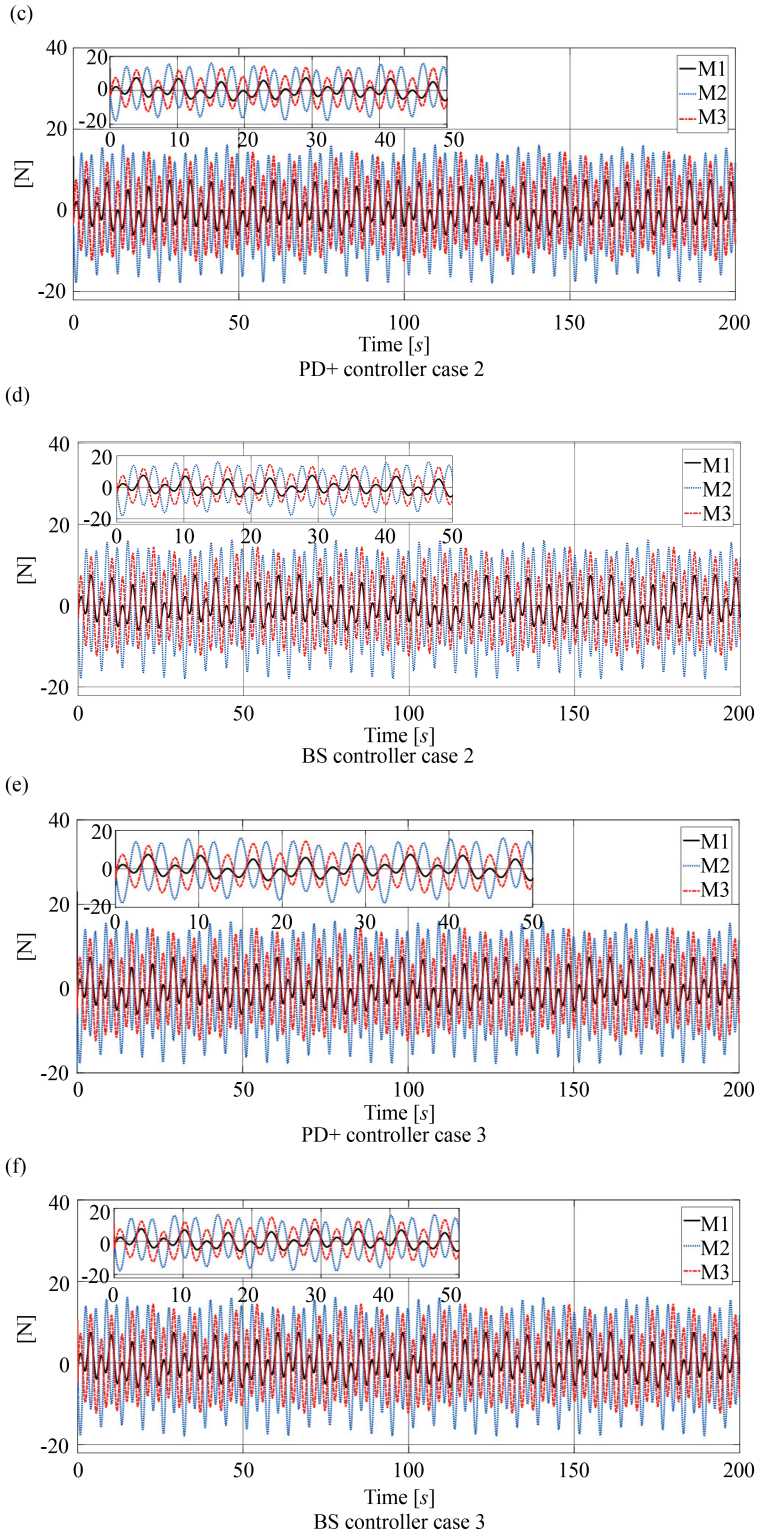

Figure 10. Graphs of the torques required by each engine generated by the control schemes

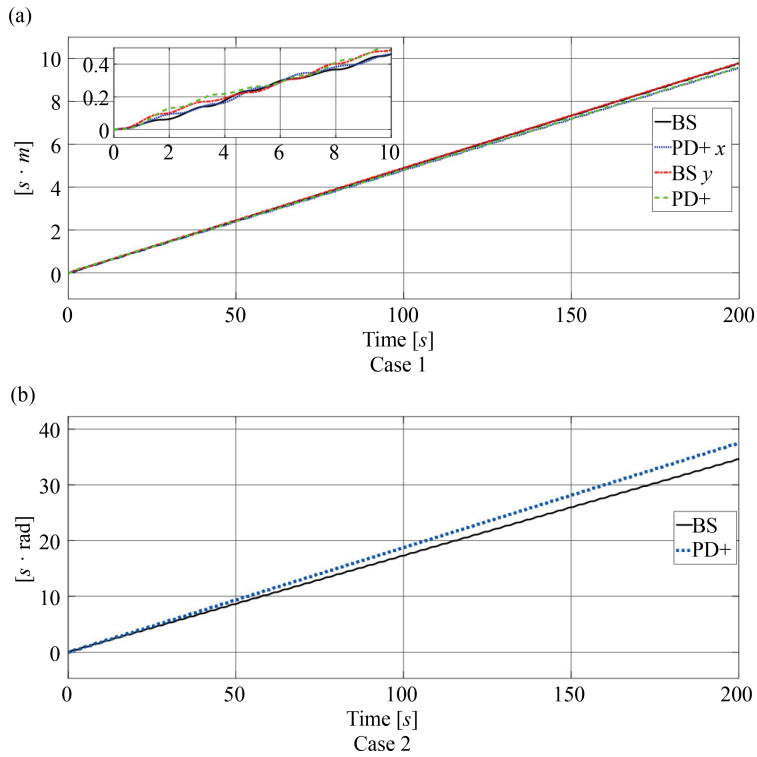

Figure 11. Evolution of the ISE of case three

On the other hand, Figures 6 and 7 show the responses of the controllers on the X and Y axes, respectively, as a function of time. It is possible that both control schemes manage to monitor trajectory presenting small oscillations around the desired trajectories, this derived from the disturbances generated by the waves and air currents. Specially in case 2, greater oscillations in the ridges in the ridges are observed Each of the axes. Similarly, Figure 8 shows the responses of the control schemes on the axis of ψ. In these graphs it can be seen that for cases one and three, there are oscillations of 0.3 rad amplitude around the desired angle. In the second case, there is a ramp-type trajectory in which the tracking is carried out with small oscillations around the desired value.

On the other hand, Figure 9 shows the graphs of the dynamics of the error generated by both control schemes for each case. In this graph it is possible to observe that both schemes generate similar dynamics that are oscillatory limited throughout the trajectory, in addition the main difference is a defass in dynamics. The above helps to show the ability to attenuate the control actions of oscillatory disturbances.

Figure 10 shows the torques resulting from the engines for each simulation, each graph indicates the torques of the three buoy engines for each controller and their study case. The torques required by both controllers for each case are similar. Furthermore, the graphs indicate that none of the three motors are in saturation and are bounded to a range of $\pm 15Nm$ and thus guarantee the system functionality with engines that meet the requirements.

From the above, the performance metrics of the Integral Error (IE), Integral of the Absolute Error (IAE), Average Square Error (ASE) and the calculation of the Total Variations of Control Efforts (TVCE), were obtained:

$$IE = \int_0^t edt, \tag{46}$$

$$IAE = \int_0^t |e|dt, \tag{47}$$

$$ASE = \frac{1}{n}\sum_1^n e^2, \tag{48}$$

$$TVCE = \sum_1^n u, \tag{49}$$

where, e is the error and n is the number of simulation samples. The final results of the error metric are shown in Table 6. On the other hand, Table 7 shows the TVCE metric. In these metric it is possible to observe that both controllers have a similar performance; however, in the X and Y coordinates the PD+ control scheme presents a slightly higher performance in the IAE and ASE metrics against the backstepping, which occurs otherwise for the coordinate of ψ. Similarly, the TVCE yield is similar for both control schemes, despite this, even backstepping control is slightly higher than PD+.

Table 6. Error metric

Case	Control schemes	IE	ME $[X,\ Y,\ \psi]$ IAE	ASE
1	PD+	[0.068, 0.046, 0.043]	[2.38, 2.39, 9.37]	[3.00, 3.00, 43.1]$x10^{-3}$
	BS	[−2.20, −1.75, 7.63]$x10^{-2}$	[2.44, 2.44, 8.61]	[3.10, 3.10, 36.8]$x10^{-3}$
2	PD+	[62.9, 14.9, −6.00]$x10^{-2}$	[9.15, 9.07, 37.55]	[3.20, 3.10, 43.5] $x10^{-3}$
	BS	[9.49, 8.70, 12.10]$x10^{-2}$	[8.63, 9.23, 34.64]	[2.90, 3.20, 37.0]$x10^{-3}$
3	PD+	[1.33, −2.27, −8.51]$x10^{-2}$	[9.57, 9.57, 37.56]	[3.00, 3.00, 43.5] $x10^{-3}$
	BS	[−6.98, −6.53, 12.1]$x10^{-2}$	[9.76, 9.75, 34.64]	[3.10, 3.00, 37.0]$x10^{-3}$

Table 7. Total variations of control efforts

Case	Control schemes	TVCE $[X,\ Y,\ \psi]$
1	PD+	[289.22, 910.60, 684.66]
	BS	[249.22, 884.12, 650.81]
2	PD+	[1,020.9, 3,554.3, 2,630.1]
	BS	[984.80, 3,545.0, 2,607.5]
3	PD+	[1,071.9, 3,589.4, 2,627.5]
	BS	[1,009.7, 3,563.0, 2,603.5]

In addition, Figure 11 shows the Integral Square Error (ISE) of Case 3, which helps to identify the performance of the controllers in each of the axes. In this way, it is possible to say that both controllers have a similar performance by having a slight variation in their final values of the ISE.

For cases 1 and 2, it is observed that the BS controller obtains a lower accumulation of error (IE) on the X, Y axes. Although in case 3, the PD+ presents a lower IAE, that is, the error along the trajectory tracking is lower; therefore, the PD+ performs better for this case.

In particular, on the ψ axis, the average error along the path (ASE) is smaller for BS, being 17% smaller compared to PD+. On the X, Y axes, PD+ shows a better performance with a difference of 3.3% with respect to BS in cases 1 and 3.

As observed in the previous paragraphs, error-based metrics show advantages in both controllers. Therefore, TVCE was used to compare the dynamics of control efforts, with which it was observed that BS requires an equivalent effort 16% lower compared to the PD+. Thus, although PD+ has better performance in the X, Y axes (cases 1 and 3), BS maintains a lower energy consumption.

6. Conclusion

The mathematical model of a BOC was developed considering the disturbances that it could have for the incident waves as well as by the wind raffles. Thus, the mathematical model is one of the main contributions of this work; because it describes a methodology to obtain it considering the disturbances of waves and wind, which directly affect the drift of the position and the stability of the attitude. The modeling of the disturbances allows to have an approach of the operation environment at the simulation level. It is important to mention that in the literature, [25] shows the mathematical model of a similar BOC; however, the model obtained in this work shows in detail each of the steps to follow to obtain it, as well as the explanation and obtaining of each parameter; also, the equations and types of disturbances are addressed in greater depth. These disturbances can be compensated by two design characteristics; a stable structure and a motion controller. It is important to highlight that the mathematical model has not been reported in any other literature, therefore, this is one of our main contributions. In addition, unlike the works that only show the value of the control actions, here the calculation to know the torque of each of the motors is described.

The designed control schemes consider the complex, non-linear dynamics and sensitivity to exogenous perturbations of the BOC. Both controllers have similar characteristics, to mention some: the need of the mathematical model, access to all system variables, arise from a stability analysis of Lyapunov and lineage the system exactly. The simulations performed show good performance of the controllers for trajectory monitoring tasks. It should be noted that both controllers, given the presence of oscillatory disturbances, exhibit a good performance by presenting a constant oscillatory error that does not significantly affect its application in the BOC despite the fact that system disturbances are not feedback to the controller. However, although PD+ performs better (based on IAE) in cases 2 and 3, BS performs better in ψ. Thus, the results obtained are interesting, as they show the results when considering the effect of waves and wind on the robot's movement, which is not usually mentioned in the literature.

It should be noted that both controllers, in the presence of oscillatory disturbances, exhibit good performance and maintain a limited steady-state error, which does not significantly affect their application in the BOC. However, based on error metrics and TVCE for the proposed tasks, backstepping is the best option. The previous conclusion is based on the fact that it is essential to have a lower error in ψ, as well as low energy consumption. Therefore, it is concluded that the methodology followed for the design of control schemes allowed obtaining control schemes that guarantee a precise and stable displacement of the buoy in the environment in which the buoy operates, this being another of the contributions of this work.

The previous results postulate the background for the implementation of autonomous buoys in maritime waters for use in various applications. Thus, the results obtained in this work serve as a basis for future research focused on the implementation of control algorithms, trajectory tracking, stability and energy consumption in experimental prototypes of autonomous buoys.

In addition, in the system implementation phase the development of control schemes could be venerated from the integration of works such as [9, 42] that would support proper engine control. Also, it is considerable to integrate articles such as [20, 21] could optimize the performance of control schemes by improving the metric and energy consumption.

Acknowledgement

This work was supported by the Secretaría de Investigación y Posgrado del Instituto Politécnico Nacional (SIP-IPN) under grants 20240039 and 20241125. All the authors thank DGAPA-UNAM for the financial support given through the PAPIIT project TA100421. Yair Lozano-Hernández is a researcher at Unidad Profesional Interdisciplinaria de Ingeniería "Alejo Peralta" (UPIIAP) and the Unidad Profesional Interdisciplinaria de Ingenieria Campus Hidalgo (UPIIH) of the Instituto Politécnico Nacional (IPN). Lizeth Torres is a researcher at the Instituto de Ingeniería of the Universidad Nacional Autónoma de México (IIUNAM). Victor G. Sanchez-Meza is enrolled in the Unidad Profesional Interdisciplinaria en Ingeniería y Tecnologías Avanzadas (UPIITA) of the IPN, where he is a Consejo Nacional de Humanidades, Ciencias y Tecnologías (CONAHCYT) fellow (CVU 964590) and is thankful for the support received. Erick Velazquez-Lozada is a researcher at the Escuela Superior de Ingenieria Mecanica y Electrica unidad Zacatenco (ESIME Zacatenco) of the IPN.

Conflict of interest

The authors declare no competing financial interest.

References

[1] Schöne T, Reigber C, Braun A. GPS offshore buoys and continuous GPS control of tide gauges. *The International Hydrographic Review*. 2003; 4: 64-70.

[2] Graber HC, Terray EA, Donelan MA, Drennan WM, Van Leer JC, Peters DB. ASIS-S new air-sea interaction spar buoy: Design and performance at sea. *Journal of Atmospheric and Oceanic Technology*. 2000; 17(5): 708-720.

[3] Farber S, Allaka H, Klein I, Groper M. Estimating sea state using a low cost buoy. In: *2018 IEEE International Conference on the Science of Electrical Engineering in Israel (ICSEE)*. IEEE; 2018. p.1-5.

[4] Vallegra F, Mateo D, Tokić G, Bouffanais R, Yue DK. Gradual collective upgrade of a swarm of autonomous buoys for dynamic ocean monitoring. In: *Oceans 2018 MTS/IEEE Charleston*. IEEE; 2018. p.1-7.

[5] Jadaliha M, Choi J. Environmental monitoring using autonomous aquatic robots: Sampling algorithms and experiments. *IEEE Transactions on Control Systems Technology*. 2012; 21(3): 899-905.

[6] Duarte M, Costa V, Gomes J, Rodrigues T, Silva F, Oliveira SM, et al. Evolution of collective behaviors for a real swarm of aquatic surface robots. *PloS One*. 2016; 11(3): e0151834.

[7] Fujii Y, Yamazoe H, Lee JH. A water sensing device control system for long-term monitoring. In: *2019 IEEE/SICE International Symposium on System Integration (SII)*. IEEE; 2019. p.572-577.

[8] Zoss BM, Mateo D, Kuan YK, Tokić G, Chamanbaz M, Goh L, et al. Distributed system of autonomous buoys for scalable deployment and monitoring of large waterbodies. *Autonomous Robots*. 2018; 42(8): 1669-1689.

[9] Koo SM, Travis H, Sands T. Impacts of discretization and numerical propagation on the ability to follow challenging square wave commands. *Journal of Marine Science and Engineering*. 2022; 10(3): 419.

[10] Menezes J, Sands T. Discerning discretization for unmanned underwater vehicles DC motor control. *Journal of Marine Science and Engineering*. 2023; 11(2): 436.

[11] Weng Y, Wang N. Data-driven robust backstepping control of unmanned surface vehicles. *International Journal of Robust and Nonlinear Control*. 2020; 30(9): 3624-3638.

[12] Zhang L, Ji X, Jiao Y, Huang Y, Qian H. Design and control of the "transboat": A transformable unmanned surface vehicle for overwater construction. *IEEE/ASME Transactions on Mechatronics*. 2022; 28(2): 1116-1126.

[13] Yin Z, Wu J, Lu Q, Zhou W. Design of small omnidirectional unmanned surface vehicle and motion control. In: *2024 6th International Conference on Electronic Engineering and Informatics (EEI)*. IEEE; 2024. p.811-815.

[14] Bignell A, Li L, Vaughan R. Open-loop collective assembly using a light field to power and control a phototaxic mini-robot swarm. In: *2019 International Conference on Robotics and Automation (ICRA)*. IEEE; 2019. p.5851-5857.
[15] Wang N, Ahn CK. Coordinated trajectory-tracking control of a marine aerial-surface heterogeneous system. *IEEE/ASME Transactions on Mechatronics*. 2021; 26(6): 3198-3210.
[16] Casavola A, El Qemmah A, Tedesco F, Torchiaro FA. Coordination of marine multi-vehicle autonomous systems via the distributed command governor approach. In: *OCEANS 2023-Limerick*. IEEE; 2023. p.1-8.
[17] Wang C, Xie S, Chen H, Peng Y, Zhang D. Course control of unmanned surface vehicle based on fuzzy sliding mode. In: *2019 IEEE International Conference on Advanced Robotics and its Social Impacts (ARSO)*. IEEE; 2019. p.287-290.
[18] Wang J, Wang J, Han QL. Neurodynamics-based model predictive control of continuous-time under-actuated mechatronic systems. *IEEE/ASME Transactions on Mechatronics*. 2020; 26(1): 311-322.
[19] Zhang Q, Pan W, Reppa V. Model-reference reinforcement learning control of autonomous surface vehicles. In: *2020 59th IEEE Conference on Decision and Control (CDC)*. IEEE; 2020. p.5291-5296.
[20] Osler S, Sands T. Controlling remotely operated vehicles with deterministic artificial intelligence. *Applied Sciences*. 2022; 12(6): 2810.
[21] Shah R, Sands T. Comparing methods of DC motor control for UUVs. *Applied Sciences*. 2021; 11(11): 4972.
[22] Yan Y, Yu S, Sun C. Event-triggered sliding mode tracking control of autonomous surface vehicles. *Journal of the Franklin Institute*. 2021; 358(8): 4393-4409.
[23] Fujii Y, Tuan Tran D, Lee JH. An efficient in situ monitoring strategy for an active aquatic surface omni-directional sensing device. *Advanced Robotics*. 2022; 36(14): 700-714.
[24] Fujii Y, Tran DT, Lee JH. Evaluation of position-keeping strategies for symmetrically-shaped autonomous water-surface robots under disturbances. In: *2022 IEEE/RSJ International Conference on Intelligent Robots and Systems (IROS)*. IEEE; 2022. p.7137-7144.
[25] Xue K, Ji X, Qu D, Peng Y, Qian H. OBoat: An agile omnidirectional robotic platform for unmanned surface vehicle tasks. *IEEE/ASME Transactions on Mechatronics*. 2023; 28(5): 2413-2424.
[26] Wang W, Shan T, Leoni P, Fernández-Gutiérrez D, Meyers D, Ratti C, et al. Roboat II: A novel autonomous surface vessel for urban environments. In: *RSJ International Conference on Intelligent Robots and Systems (IROS)*. IEEE; 2020. p.1740-1747.
[27] Lončar I, Babić A, Arbanas B, Vasiljević G, Petrović T, Bogdan S, et al. A heterogeneous robotic swarm for long-term monitoring of marine environments. *Applied Sciences*. 2019; 9(7): 1388.
[28] Wang W, Mateos LA, Park S, Leoni P, Gheneti B, Duarte F, et al. Design, modeling, and nonlinear model predictive tracking control of a novel autonomous surface vehicle. In: *2018 IEEE International Conference on Robotics and Automation (ICRA)*. IEEE; 2018. p.6189-6196.
[29] Fossen TI. *Handbook of Marine Craft Hydrodynamics and Motion Control*. Trondheim, Norway: John Wiley and Sons; 2011.
[30] Fossen TI. *Guidance and Control of Ocean Vehicles*. Trondheim, Norway: John Wiley and Sons; 1999.
[31] Lindegaard KP. *Acceleration Feedback in Dynamic Positioning*. Trondheim, Norway: Fakultet for Informasjonsteknologi, Matematikk Og Elektroteknikk; 2003.
[32] Imlay FH. *The Complete Expressions for Added Mass of a Rigid Body Moving in an Ideal Fluid*. David Taylor Model Basin Washington DC; 1961.
[33] Newman JN. *Marine Hydrodynamics*. London, England: The MIT; 2018.
[34] Kaneko S, Nakamura T, Inada F, Kato M, Ishihara K, Nishihara T, et al. Vibrations in fluid-structure interaction systems. In: *Flow-induced Vibrations (Second Edition)*. Oxford: Academic Press; 2014. p.359-401.
[35] Balanza L, Claudia DLC. *Modelado Dinámico Del Barco De Pequeño Porte Krick Felix [Dynamics Modeling of Crick Felix Small Ship]*. Universidad Central "MartaAbreu" De Las Villas; 2017.
[36] Vázquez J, Velasco-Villa M. Path-tracking dynamic model based control of an omnidirectional mobile robot. *IFAC Proceedings Volumes*. 2008; 41(2): 5365-5370.
[37] Ordóñez-Hurtado RH, Duarte-Mermoud MA. Finding common quadratic Lyapunov functions for switched linear systems using particle swarm optimisation. *International Journal of Control*. 2012; 85(1): 12-25.
[38] Saberi A, Khalil H. Quadratic-type Lyapunov functions for singularly perturbed systems. *IEEE Transactions on Automatic Control*. 1984; 29(6): 542-550.

[39] Ibarra EG, Lozano Hernández Y, Enríquez MA, Galván Guerra R, Maya MC. Super-Twisting Control for trajectory tracking of a four-degree of freedom anthropomorphic robot manipulator. *Nova Scientia*. 2022; 14(28). Available from: https://doi.org/10.21640/ns.v14i28.2723.

[40] Bouabdallah S, Siegwart R. Backstepping and sliding-mode techniques applied to an indoor micro quadrotor. In: *Proceedings of the 2005 IEEE International Conference on Robotics and Automation*. IEEE; 2005. p.2247-2252.

[41] Ginanjar S, Adiningsih S, Fadlilah Y, Wulandari S, Petrova C, Ikhtiarino S. Coastal storm waves detection system design using Beaufort scale standardization and Sugianto wave forecasting method in Timbulsloko, Demak, Central Java, Indonesia. In: *IOP Conference Series: Earth and Environmental Science*. IOP Publishing; 2021. p.012066.

[42] Wang L, Pang S. Autonomous underwater vehicle based chemical plume tracing via deep reinforcement learning methods. *Journal of Marine Science and Engineering*. 2023; 11(2): 366.